A novel method to measure the sagittal curvature in spinal deformities: the reliability and feasibility of 3D ultrasound imaging

Corresponding author: Check the box beside to identify the corresponding author.

☐ Timothy Tin-Yan Lee, M.Phil.
Department of Biomedical Engineering, The Hong Kong Polytechnic University, Hong Kong SAR, China
11900911r@connect.polyu.hk

☐ Connie Lok Kan Cheng, M.Phil.
Department of Biomedical Engineering, The Hong Kong Polytechnic University, Hong Kong SAR, China
connie.0912@connect.polyu.hk

☐ René M. Castelein, M.D., Ph.D.
Department of Orthopaedic Surgery, University Medical Center Utrecht, Utrecht, The Netherlands
r.m.castelein@umcutrecht.nl

√ Jason Pui Yin Cheung, M.B.B.S.
Department of Orthopaedics and Traumatology, The University of Hong Kong, Hong Kong SAR, China
jcheung98@hotmail.com

☐ Wei Wei Jiang, Ph.D
College of Computer Science and Technology, Zhejiang University of Technology, Hangzhou, China
jamie.jww@connect.polyu.hk

☐ Kelly Ka-Lee Lai, B.Eng.
Department of Biomedical Engineering, The Hong Kong Polytechnic University, Hong Kong SAR, China
kelly.lai@polyu.edu.hk

☐ Michael Kai Tsun To, M.B.B.S.
Department of Orthopaedics and Traumatology, The University of Hong Kong, Hong Kong SAR, China
michaelktto@ortho.hku.hk

☐ Yong-Ping Zheng, Ph.D.
Department of Biomedical Engineering, The Hong Kong Polytechnic University, Hong Kong SAR, China
yongping.zheng@polyu.edu.hk

*Jason Pui Yin Cheung, MBBS, MMedSc,
MS, PDipMDPath, FHKCOS, FHKAM, FRCSEd,
Department of Orthopaedics and Traumatology,
The University of Hong Kong, Pokfulam, Hong Kong, China.
E-mail: cheungjp@hku.hk

A novel method to measure the sagittal curvature in spinal deformities: the reliability and feasibility of 3D ultrasound imaging

ABSTRACT

The objective of this study is to test the reliability of sagittal spinal curvature measurements using three-dimensional (3D) ultrasound in adolescent idiopathic scoliosis (AIS) patients. Ultrasound spinous process angle (USSPA) and ultrasound laminae angle (USLA) were measured on sagittal ultrasound images, while Cobb angle (XCA) was measured on sagittal X-ray images. Intraclass correlation coefficients (ICC) for the intra- and inter-observer variability, linear regression analysis and Bland-Altman method including mean absolute difference (MAD) were investigated to evaluate the reliability and validity of the two ultrasound angles as compared to XCA. Excellent measurement reliabilities were demonstrated for both ultrasound angles (ICC≥0.91). Moderate to good and significant linear correlations and good agreement were demonstrated between the ultrasound methods and XCA (Thoracic ($R^2 \geq 0.574$) / Lumbar ($R^2 \geq 0.635$)). No significant differences were found from the MADs between both corrected ultrasound angles and XCA. Sagittal ultrasound angles demonstrated to be reliable for assessing sagittal curvature using spinous processes and laminae, and have good and significant correlations with Cobb angles. Since it is non-ionizing and relatively low cost, this opens the possibility to provide frequent curve monitoring and evaluation, and screening for AIS patients, particularly based on sagittal profiles.

Keywords: 3D ultrasound; Scoliosis; Sagittal; Spinous processes

INTRODUCTION

Idiopathic scoliosis is a three-dimensional (3D) deformity characterized by lateral deviation, sagittal misalignment and transverse axial rotation of the spine (Pope et al. 1984). Among all paediatric spine deformities, adolescent idiopathic scoliosis (AIS) is most prevalent (Cheng et al. 2015; Fong et al. 2015; Tambe et al. 2018). Whereas in the past, the coronal plane deformity has received most attention, it has become clear that the sagittal plane in AIS is at least as important, both in analyzing the overall deformity, as in establishing treatment goals (Cheng et al. 2015; Post et al. 2019). In clinical practice, the traditional standard for evaluating the sagittal profile is by the sagittal Cobb angle (Cobb 1948). However, due to the effect of coupling in different planes, the pattern of deformity in the sagittal plane may be highly influenced and distorted by changes in the other two planes (Hayashi et al. 2009, Sullivan et al. 2017). Different coronal curve patterns are characterized by differences in sagittal profile, and these also differ from normal spines (Schlösser et al. 2014). Quantifying spinal curvatures in different planes is useful for preoperative planning, postoperative evaluation and monitoring curve progression (Cheung et al. 2013; de Bodman et al. 2017, Vrtovec et al. 2009, Post et al 2019) but there are significant limitations with using only two-dimensional posteroanterior and lateral radiographs for evaluating scoliosis.

Free-hand 3D ultrasound, combining conventional B-mode ultrasound images with spatial sensing (Huang et al. 2005), is relatively cheap and becoming more popular. Different from X-ray, the gold standard imaging modality for evaluating AIS patients, ultrasound is radiation-free. In addition, in some countries physiotherapists were not authorized to request X-ray examination (de Oliveira et al. 2012). 3D ultrasound was first explored on AIS patients by Suzuki et al. (1989), by combining the transducer with an attached inclinometer to measure coronal Cobb angle and vertebrae rotation. Later on, ultrasound has been demonstrated to be feasible to examine posterior vertebrae morphology (Chin et al. 2011; Darrieutort-Laffite et al. 2014; Salman et al. 2011). Li et al. (2012) investigated the effectiveness of orthotic treatment for patients with AIS using 3D ultrasound in terms of spinous process angle in order to enhance the effectiveness of orthotic treatment. The results showed that the ultrasound-assisted fitting method of spinal orthosis was effective and beneficial to 62 % of the patients. Other than spinous process angle, center of lamina method had also been used for ultrasound to evaluate coronal curvature. This method also showed high intra- and inter-rater reliability and moderate correlation with X-ray Cobb (Young et al. 2015). Wang et al. (2015) further investigated the reliability and validity of this method in clinical setting by comparing to the corresponding MRI measurement on 16 patients with AIS, and similarly high intra- and inter-rater reliability were demonstrated and no significant difference were observed between the ultrasound results and MRI Cobb. Furthermore, tracked ultrasound had been utilized to localize vertebral transverse processes to measure curvature angles on spine phantoms, and close correlation was found between the tracked ultrasound transverse process angle and the radiographic Cobb measurements with small inter-operator differences (Ungi et al. 2014).

A 3D ultrasound imaging method was developed and preliminary tests were conducted on flexible spinal column phantoms (Cheung et al. 2013) and human subjects (Cheung et al. 2015). Ultrasound measurements were performed were found to have good linear correlation with X-ray and Bland-Altman showed good agreement between ultrasound and X-ray in both studies. The ultrasound system was further modified and improved, and eventually became the 3D ultrasound imaging system used in this study. It was demonstrated to provide results excellent intra- and inter-rater and operator reliability, and moderate to strong correlation with Cobb's angle in previous study (Zheng et al. 2016), where the results correlated better than Quantec system (R^2 = 0.66)

(Goldberg et al. 2001) and the Orthoscan system (R^2 = 0.42) (Knott et al. 2006). The reliability and validity of different coronal spinal ultrasound angle measurements were further investigated using the same ultrasound system, excellent correlations were found between ultrasound and Cobb measurement and no differences in reliability and validity were observed between the ultrasound angles based on the spinous processes and transverse processes (Brink et al. 2018). The 3D ultrasound system were also demonstrated to provide reliable information of spinal flexibility and in-orthosis correction of patients with AIS in the prone position (He et al. 2017) and the patterns of alternation of coronal curve changes of patients with AIS during forward bending (Jiang et al. 2018). In a previous study, ultrasound was shown to be able to provide reliable sagittal measurement of spinal phantoms and a few human subjects (Lee et al. 2019), however the sample size of the human subjects was too small and relatively long period was required for data acquisition. In addition, laminae were observed to be more obvious than spinous processes in ultrasound images for providing reliable landmarks for measurement. As such, the aim of this study is to investigate the utility of 3D ultrasound for measuring the sagittal curvatures with a larger number of AIS subjects, using spinous processes and laminae as landmarks for measurement, respectively.

METHODS

Subjects

Patients diagnosed with AIS were recruited from a tertiary scoliosis referral center to participate in this study. Patients were requested to receive both ultrasound scanning and X-ray imaging on the same day. This study was approved by the local institutional review board. Signed informed consents were obtained from all subjects and their parents/guardians. Patients with Cobb angle larger than 50 degrees, metallic implants and body mass index (BMI) greater than 25.0 kg/m^2 were excluded, as metallic implants would affect the spatial sensing accuracy of the ultrasound probe and high BMI would likely lead to poor image quality in the lumbar region. Patients who were wearing a brace during x-rays or allergic to ultrasound gel were excluded.

3D ultrasound system

The spine scanning was achieved using the 3D ultrasound imaging system (Figure 1a), Scolioscan®, (Scolioscan, Model SCN801, Telefield Medical Imaging Ltd, Hong Kong) and EOS® system (EOS® imaging, Paris, France) which is a bi-planar X-ray imaging system that generates upright images of the spine with less radiation and allows 3D spine modeling (Deschênes et al. 2010; Glaser et al. 2012). The specification of the 3D ultrasound system and the testing protocol on human subjects had been reported in a previous study (Zheng et al. 2016). Linear ultrasound probe (frequency of 7.5 MHz, width of 7.5 cm) was used for freehand ultrasound scanning of the spine, with a spatial sensor attached to detect the position and orientation of the probe. Supporters on the chest and hip boards of the ultrasound system, which were adjusted to a patient specific height and length, were positioned to align with clavicle anterior concavities bilateral anterior superior iliac spines respectively to stabilize the patients during the scanning process in a natural standing position (Figure 1b). In addition, patients were asked to keep their eye level horizontal at the level of the eye-spot shown on the patient screen and to focus on the spot throughout the scanning process. Warmed aqueous ultrasound gel was applied to the patient's back by the operators to fill the spinal furrow and to cover the extent of where the probe would sweep. Pre-scanning was performed along L5 and T1, and corresponding adjustment of time gain constant and brightness for B-mode image was conducted to achieve an overall good image quality for the scanning region. After setting the scanning range, the scanning of the spine was conducted by controlling the probe manually, and started approximately from the L5 level and continued to go upward along the spine to the C7 level. The scanning procedure takes approximately 30 seconds. After scanning, the collected B-mode image together with the corresponding orientation and position recorded were used for 3D ultrasound volume reconstruction, and the volumes were then transferred to a customized software for post-processing and generating sagittal ultrasound images for measuring the sagittal curvature. Coronal ultrasound images were automatically formed by obtaining an averaged intensity of all voxels of the ultrasound volume within a selected depth of approximately 10 mm along the anteroposterior direction and using a non-planar re-slicing technique using the skin surface as a reference for selecting the required voxels. The coronal ultrasound angle(s) were measured by manually drawing the lines on the most tilted part of the mid-line on the coronal image, which represents the shadow of the spinous processes (Figure 2), and has been demonstrated to be reliable and repeatable (Brink et al. 2018, Zheng et al. 2016). Since surface references were not available for generating sagittal ultrasound images, they were formed by transferring the ultrasound volume to a customized software and manually selecting the suitable slices along the medial-lateral direction, where the spinous processes and bilateral laminae could be visualized.

Data collection

Two operators and three raters were involved to conduct US scanning and angle measurements respectively Rater 1 and Rater 2 were responsible to conduct ultrasonic measurements, who were novice researchers with more than 2 years of experience in studying the human spine using 3D ultrasound. Rater 3 was a spine surgeon responsible for radiographic Cobb angle measurements.

For ultrasound, thoracic kyphosis and lumbar lordosis were measured by the spinous process angle (USSPA) and the laminae angle (USLA). To compute USSPA and USLA, three sagittal ultrasound images visualizing the spinous processes (Figure 3a) and bilateral laminae (Figure 3b) were first manually obtained by Rater 1 using a customized 3D ultrasound software. This procedure had been repeated twice to generate two sets of images for each subject by Rater 1. The centre of spinous processes and laminae were considered as the landmarks for measuring USSPA and USLA. Thoracic USSPA was defined by the intersection angle between the line joining T3 and T4 spinous processes and the line joining T11 and T12 spinous processes, whereas lumbar USSPA was defined by the intersection angle between the line joining T12 and L1 spinous processes and the line joining L4 and L5 spinous processes (Figure 4a). USLA was defined by the average of the angle values obtained from the left and right laminae. Thoracic USLA was defined by the averaged intersection angle between the line joining T3 and T4 (left/right) laminae and the line joining T11 and T12 (left/right) laminae, whereas lumbar USLA was defined by the intersection angle between the line joining T12 and L1 (left/right) laminae and the line joining L4 and L5 (left/right) laminae (Figure 4b). Both measurements were performed using RadiAnt DICOM Viewer software (Medixant, Poland). Approximate levels of T3, T12 and L5 were indicated by Rater 2 on the sagittal ultrasound image to avoid line misplacement on specific vertebral landmarks.

Thoracic XCA was defined by the angle formed by the upper endplate of T4 vertebra and the lower endplate of the T12 vertebra, whereas lumbar XCA was defined by the angle formed by the upper endplate of L1 vertebra and the lower endplate of the L5 vertebra from the standing posteroanterior X-ray images by Rater 3 (Figure 4c) (Boseker et al. 2000). All raters performed the measurement independently and were blinded to the patients' details.

Statistical Analysis

Statistical analysis was conducted using SPSS Version 20.0 (IBM, SPSS Inc., USA) software. Intra-class coefficient (ICC) was calculated to evaluate the reliability between the measurements of the raters. For the intra-rater reliability, two measurements acquired from the same sagittal image were compared individually by each rater (Shrout and Fleiss 1979). For the inter-rater reliability, the first measurement results of the two raters were compared (Shrout and Fleiss 1979). In order to test the reliability of the generating procedure of the sagittal image, two sets of sagittal ultrasound angles, measured by Rater 1, each from different ultrasound sagittal images generated using the customized 3D software from the same scan, were compared. The Currier criteria for evaluating ICC values were adopted: very reliable (0.80–1.0), moderately reliable (0.60–0.79), and questioned reliable (≤0.60) (Currier 1984). Ultrasound measurements were compared with XCA respectively using linear correlation for thoracic curves and lumbar curves. Linear regression equations with intersections were analyzed with correlation coefficients 0.25 to 0.50 indicating poor correlation, 0.50 to 0.75 indicating moderate to good correlation, and 0.75 to 1.00 indicating very good to excellent correlation (Dawson and Trapp 2004). Adjusted ultrasound angles were then computed by substituting the ultrasound angles into the regression equation obtained. Bland-Altman method was used to test the agreement between XCA and the adjusted ultrasound angles, based on the results obtained by Rater 1. Mean absolute differences (MAD) between XCA and the adjusted ultrasound angles were calculated and were compared using paired t-tests. The significance level was set at 0.05.

RESULTS

A total of 21 patients (14 females) with mean age of 15.7 ± 1.3 years (range 12-18 years) were included in this study. 2 patients had to be excluded since USSPA could not be measured due to insufficient imaging quality caused by poor contact surface of the skin of skinny subjects. The mean coronal Cobb angle was 24.5 ± 9.0° (range 11.1 – 41.9°), which was evaluated by the angle formed between lines drawn on the most tilted upper vertebral endplate and lower vertebral endplate of coronal curves. Thoracic and lumbar sagittal XCAs were on average 22.7 ± 14.0° (range 0.7 – 44.6°) and 38.0 ± 12.6° (range 14.7 – 60.0°) respectively. Thoracic and lumbar sagittal ultrasound angles were on average 28.1 ± 10.4° and 18.5 ± 9.2° (USSPA) and 34.6 ± 10.5° and 26.5 ± 12.0° (USLA).

Excellent reliabilities were obtained for both ultrasound angles in both thoracic and lumbar regions from the same set (Table 1) and different set of images (Table 2). Both USSPA (Figure 5a) and USLA (Figure 5b) showed moderate to good linear correlations with XCA. Thoracic USLA was found to have the lowest R^2 value (0.574), while lumbar USLA was found to have the highest R^2 value (0.701). The Bland-Altman plot showed a good agreement between the ultrasound angles adjusted with the linear equations and the XCA (Figure 6a and 6b). No significant difference was found between both adjusted ultrasound angles (MAD: USSPA 6.4 ± 4.8° / 6.1 ± 4.4°; USLA 7.5 ± 4.9° / 5.3 ± 4.2°; $p \geq 0.326$ for thoracic / lumbar curves respectively).

DISCUSSION

The importance of the sagittal plane of the spine has become well recognized. Traditionally, sagittal curvature of spine is evaluated by radiographic Cobb angle, which necessitates ionizing radiation to form the images. Alternative imaging modalities have been suggested to minimize or avoid the radiation issue. Bi-planar stereoradiography utilizes lower dosage of radiation, but it is expensive and not readily available to most medical practitioners. Ultrasound imaging is non-ionizing and relatively cheap, and has the potential of wide spread use and screening purposes. During ultrasound scanning, subjects are maintained in the upright posture, same as that adopted during traditional radiographic examination, thereby providing a real alternative to erect X-ray images. But since ultrasound scanning is conducted on the back of the subjects, only posterior structures of the vertebrae can be seen from the ultrasound images, thus landmarks like spinous processes and bilateral laminae were used for sagittal spine measurement instead of vertebral endplates in this study. Previous study has demonstrated the possibility of ultrasound to assess the sagittal spinal curvature on spinal phantoms (Lee et al. 2019), and this paper further validates the reliability and validity of studying the sagittal plane, using different sagittal angle measurement methods using ultrasound. Excellent intra- and inter-rater reliabilities were demonstrated for ultrasound sagittal angle measurement, and good to moderate linear correlations were demonstrated between the ultrasound angles and radiographic Cobb angles. The average MAD of the corrected ultrasound measurements was about 6.3°, without significant difference between the different ultrasound measurements. Since the maximum measurement error on X-ray images was found to be 6 degrees (Prujis et al. 1994), the ultrasound results obtained in this study were sufficient for clinical use. The MADs were higher in the thoracic region for both ultrasound methods and were probably due to the instability of the patients to maintain the posture during scanning, since scanning initiated from the lumbar to the thoracic region and longer time was needed to scan the thoracic region.

There is a difference between the US and X-Ray measurements. The sagittal ultrasound angles obtained were larger in the thoracic curves and smaller in the lumbar curves as compared to their corresponding sagittal radiographic Cobb angles. There were several possible reasons for the discrepancies: 1) The ultrasound measurements were based on spinous processes and bilateral laminae, which are structures located more posteriorly than the vertebral body, which is where Cobb angle is by definition measured (Brink et al. 2018). Differences in structures used for measurements thus will possibly lead to a different projection of the 3D deformity (Herzenberg et al. 1990). In addition, it has been found that measurements based on posterior vertebral structures would cause the angular value differences (Appendix B) (Chernukha et al. 1998); 2) Different positions of arms were adopted for different imaging modalities. Patients were in a relaxed standing posture with arms at the sides for ultrasound, whereas arms were bent with fists overlying ipsilateral clavicles was the adopted position for X-ray scanning respectively (Pasha et al. 2016). Decrease in kyphosis and increase in lordosis were observed when patients adopted the fists overlying ipsilateral clavicles position compared to relaxed standing (Marks et al. 2009); 3) Different levels of vertebrae were involved for X-ray and ultrasound assessments due to different measurement techniques. To conduct sagittal measurements, lines were drawn on upper or lower endplates and adjacent spinous processes and laminae on X-ray images and ultrasound images respectively, hence an extra level was involved for every line drawn on ultrasound images. To achieve consistency on the level selection, the spinous process or laminae of the superior vertebrae were involved during sagittal measurement on ultrasound images. Thus T3 and T4 were involved for constructing the superior line for thoracic curvature measurement in ultrasound images, which possibly lead to a larger value of the thoracic ultrasound angle (Appendix B). Usually, on standard X-Ray, it is difficult to obtain a clear image of any vertebra higher than T4 due to over-projection of the shoulders, which is not a problem in ultrasound. We should bear in mind that using traditional Cobb angles alone is not sufficient to comprehensively study the complex 3D deformity of scoliosis. In addition, sagittal ultrasound images formed in this study are based on the projection of the spinous process or bilateral laminae selected in the 3D ultrasound volume. This reflects a real sagittal profile of that segment of the scoliotic spine, rather than the projection of a twisted structure on a lateral radiograph, which is influenced by vertebral rotation and magnitude of deformity.

It has been known that radiographic evaluation requires the use ionizing radiation, which was especially harmful to children during puberty (Cheung et al. 2016). Repeated radiation exposure may increase the risk of breast and endometrial cancer in female AIS patients (Doody et al. 2000, Ronckers et al. 2010, Simony et al. 2016) and contribute to leukaemia and prostate cancer in adolescents (Schmitz-Feuerhake et al. 2011). Though bi-planar stereoradiography provides coronal and sagittal X-ray images with reduced radiation dosage and can be used to reconstruct the 3D spine deformity with customized reconstruction software (Al-Aubaidi et al. 2013), biplanar x-ray is not readily available for all healthcare providers due to its high cost and requiring a large area for installation (McKenna et al. 2012). In addition, relatively large difference in accuracy was found between the anterior and the posterior vertebral regions, since several anatomical landmarks on the posterior arch such as the transverse and/or spinous processes may be barely visible on the X-ray images, which caused reconstruction error leading to discrepancies (Mitulescu et al. 2002). In addition, the time needed to reconstruct a detailed 3D spine model was an average of 20 to 30 minutes, and cases with a severe scoliotic curve would definitely require a significantly longer time (Somoskeöy et al. 2012), which was not feasible under routine clinical circumstances. Magnetic resonance imaging (MRI) and computed tomography (CT) are also common for investigating scoliotic spine in the clinical and research fields. However, both MRI and CT are costly and less accessible (Diefenbach et al. 2013). In addition, MRI requires expertise to operate with long acquisition time, whereas CT requires a higher amount of radiation dosage than traditional radiograph. Most importantly, patients are required to be assessed in supine position. Different anthropometric tools have been used to evaluate sagittal spinal curvature such as stero camera (Goldberg et al. 2001), 3D digitizer (Salem et al. 2015), reflective skin markers (Schmid et al. 2015), inclinometers (Lewis et al. 2010), adapted arcometer (Chaise et al. 2011), spinal mouse (Mannion et al. 2004). However, these methods were either not precise enough or requires a long period for palpation. Moreover, the above methods only consider the back topography, but not the actual spinal anatomy.

We observed that sagittal curvature analysis using ultrasound requires a higher demand on scanning and image quality control than that of coronal curvature analysis, because sagittal measurements were required to be conducted directly on vertebrae structures, instead of just measuring the spinous process shadow for coronal curvatures measurement. In addition, patients with high BMI were not included in the study as the ultrasound frequency used has been mostly attenuated and could not reach the vertebrae structure. Hence additional attention should be paid in the future during scanning, such as using lower frequencies ultrasound probes, especially for patients with a lumbar curves in order to capture the vertebral structures since they are deeper from the skin surface. In addition, sagittal images were needed to be generated manually using the customized software. Such process required a certain degree of expertise in viewing ultrasound and spine anatomy, thus the inter-rater reliability of sagittal image generation could not be tested in this study. Age and BMI might be confounding factors that possibly affect the sagittal parameters, however we think that it may not be necessary to adjust the angle measurements for such factors in this study as no significant correlation has been observed between these factors and the sagittal angles. In addition, the patients included in this study has similar ages (small standard deviation) and BMI < 25, thus we think our results are suitable enough to reflect the real situation, though the effect of BMI on the quality of the ultrasound images requires to be explored in future study. Patients with Cobb angles larger than 50 degrees were excluded in this study since spinal sagittal measurement can be prone to measurement error due to the presence of severe rotation (Bao et al. 2018). 2 subjects had been further excluded in this study because the appearance of the spinous processes in the ultrasound images of some patients would somehow be affected for very skinny patients, due to the protruded scanning trajectories when their backs were being scanned. This problem could be tackled by applying a large ultrasound gel pack at the back of these patients in future studies. However, the laminae would not be affected due to the above issue, thus USLA measurement is more preferable when these patients are being assessed in future study. Since the MADs of the two ultrasound angles were not significantly different, the USLA should be used to overcome this issue for future study. Nevertheless, this study showed that for this scoliotic population, sagittal curvature of the spine can be evaluated using the 3D ultrasound system, either using spinous processes or bilateral laminae. Future studies with larger number of both scoliotic and non-scoliotic subjects are worthwhile to be conducted to further verify the correlation between the results of ultrasound and X-ray measurements.

CONCLUSIONS

This is the first study to report the feasibility of using ultrasound to assess the sagittal curvature of human scoliotic spines, based on images obtained by the spinous processes and laminae. In this study, we found moderate to good correlations between the ultrasound and Cobb angles, and similar results of reliability and validity were found between the two ultrasound angles. The differences in angle values can be explained by the different structures used for measurement, and by the fact that ultrasound offers the possibility to assess in the true sagittal plane of the studied spinal segment using the 3D ultrasound software. AIS is a 3D deformity and thus the true sagittal profile is not well delineated by a simple 2D X-ray due to the coupling that occurs between the deformations in the three planes. In this study, three-dimensional ultrasound is suggested as a new, non-ionizing technique to provide the real sagittal and coronal profile in an upright, unforced position.

ACKNOWLEDGEMENTS

Dr. Zheng reports grants and other from Telefield Medical Imaging Limited, outside the submitted work. In addition, Dr. Zheng has patents "A three-dimensional (3D) ultrasound imaging system for assessing scoliosis. Patent issued: US 8,900,146 B2; China 201080040696.0; Japan 5849048. Pending in Canada, Australia, and EU. Filled in Jul 2009"; " Method and device for 3D ultrasound imaging. Chinese patent. No. 200810094381.9. Filed in Apr 2008"; "Rapid 3D ultrasound measurement. Chinese patent issued. No. ZL 200510127193.8. Mar 18 2009". with royalties paid to The Hong Kong Polytechnic University by Telefield Medical Imaging Limited. In addition, Dr. Zheng has following patent pending: "Imaging method and device. PCT/CN2016/080261; Filed in Apr 2016", "Method and device for measuring spinal column curvature. PCT/CN2016/080159. Filed in Apr 2016. "Medical imaging system with mechanical arm. PCT/CN2014/085196; Filed in Aug 2014."

REFERENCES LIST

Al-Aubaidi Z, Lebel D, Oudjhane K, Zeller R. Three-dimensional imaging of the spine using the EOS system: is it reliable? A comparative study using computed tomography imaging. J Pediatric Orthopaedics B, 2013;22:409–412.

Bao H, Liu Z, Bao M, Zhu Z, Yan P, Liu S, Feng Z, Qian B, Qiu Y. Predicted final spinal height in patients with adolescent idiopathic scoliosis can be achieved by surgery regardless of maturity status. Bone Joint J. 2018;100-B(10):1372-1376.

Boseker EH, Moe JH, Winter RB, Koop SE. A determination of the normal thoracic kyphosis: a roentgenographic study of 121 normal children. J Pediatr Orthop. 2000; 20:796–798.

Brink RC, Wijdicks SPJ, Tromp IN, Schlösser TPC, Kruyt MC, Beek FJA, Castelein RM. A reliability and validity study for different coronal angles using ultrasound imaging in adolescent idiopathic scoliosis. Spine J. 2018;18(6):979-985.

Chaise FO, Candotti CT, Torre ML, Furlanetto TS, Pelinson PP, Loss JF. Validation, repeatability and reproducibility of a noninvasive instrument for measuring thoracic and lumbar curvature of the spine in the sagittal plane. Rev Bras Fisioter. 2011;15(6):511-517.

Chen W, Lou EH, Zhang PQ, Le LH, Hill D. Reliability of assessing the coronal curvature of children with scoliosis by using US images. J Child Orthop. 2013;7(6):521–529.

Cheng JC, Castelein RM, Chu WCC, Danielsson AJ, Dobbs MB, Grivas TB, Gurnett CA, Luk KD, Moreau A, Newton PO, Stokes IA, Weinstein SL, Burwell RG. Adolescent idiopathic scoliosis. Nat Rev Dis Primer. 2015;1:15068.

Chernukha KV, Daffner RH, Reigel DH. Lumbar lordosis measurement. A new method versus Cobb technique. Spine. 1998;23(1):74–79.

Cheung CW, Law SY, Zheng YP. Development of 3-D US system for assessment of adolescent idiopathic scoliosis (AIS): and system validation. Conf Proc IEEE Eng Med Biol Soc. 2013;6474–6477.

Cheung CW, Zhou GQ, Law SY, Mak TM, Lai KL, Zheng YP. Ultrasound Volume Projection Imaging for Assessment of Scoliosis. IEEE Trans Med Imaging. 2015;34(8):1760–1768.

Cheung CWJ, Zhou GQ, Law SY, Lai KL, Jiang WW, Zheng YP. Freehand 3D ultrasound system for assessment of scoliosis. JOT. 2015;3(3):123–133.

Cheung JP, Cheung PW, Samartzis D, Cheung KM, Luk KD. The use of the distal radius and ulna classification for the prediction of growth: peak growth spurt and growth cessation. Bone Joint J. 2016 Dec;98-B(12):1689-1696.

Chin KJ, Karmakar MK, Peng P. Ultrasonography of the adult thoracic and lumbar spine for central neuraxial blockade. Anesthesiology. 2011;114(6):1459–1485.

Cobb JR. Outline for the study of scoliosis. In: American Academy of Orthopaedic Surgeons, Instructional Course Lectures. St Louis: CV Mosby; 1948:261–275.

Currier DP. Elements of research in physical therapy. 3rd edn. Williams & Wilkins, Baltimore; 1984.

Darrieutort-Laffite C, Hamel O, Glémarec J, Maugars Y, Le Goff B. Ultrasonography of the lumbar spine: sonoanatomy and practical applications. Joint Bone Spine. 2014;81(2):130–136.

Dawson B, Trapp RG. Basic and Clinical Biostatistics. 4th ed. New York: McGraw-Hill Professional; 2004.

de Bodman C, Miyanji F, Borner B, Zambelli PY, Racloz G, Dayer R. Minimally invasive surgery for adolescent idiopathic scoliosis: correction of deformity and peri-operative morbidity in 70 consecutive patients. Bone Joint J. 2017;99-B(12):1651-1657.

de Oliveira TS, Candotti CT, La Torre M, Pelinson PP, Furlanetto TS, Kutchak FM, Loss JF. Validity and reproducibility of the measurements obtained using the flexicurve instrument to evaluate the angles of thoracic and lumbar curvatures of the spine in the sagittal plane. Rehabil Res Pract. 2012:186156.

Deschênes S, Charron G, Beaudoin G, Labelle H, Dubois J, Miron MC, Parent S. Diagnostic imaging of spinal deformities reducing patients radiation dose with a new slot-scanning X-ray imager. Spine. 2010;35:989–994.

Diefenbach C, Lonner BS, Auerbach JD, Bharucha N, Dean LE. Is radiation-free diagnostic monitoring of adolescent idiopathic scoliosis feasible using upright positional magnetic resonance imaging? Spine 2013;38:576–580.

Doody MM, Lonstein JE, Stovall M, Hacker DG, Luckyanov N, Land CE. Breast cancer mortality after diagnostic radiography: findings from the U.S. Scoliosis Cohort Study. Spine. 2000;25(16):2052–2063.

Fong DYT, Cheung KMC, Wong YW, Wan YY, Lee CF, Lam TP, Cheng JC, Ng BK, Luk KD. A population-based cohort study of 94401 children followed for 10 years exhibits sustained effectiveness of scoliosis screening. Spine J. 2015;15:825–833.

Glaser DA, Doan J, Newton PO. Comparison of 3-dimensional spinal reconstruction accuracy: biplanar radiographs with EOS versus computed tomography. Spine. 2012;37(16):1391–1397.

Goldberg CJ, Kaliszer M, Moore DP, Fogarty EE, Dowling FE. Surface topography, Cobb angles, and cosmetic change in scoliosis. Spine 2001; 26(4):E55-63

Harrison DD, Janik TJ, Troyanovich SJ, Holland B. Comparisons of lordotic cervical spine curvatures to a theoretical ideal model of the static sagittal cervical spine. Spine 1996;21(6):667-75.

Hayashi K, Upasani VV, Pawelek JB, Aubin CE, Labelle H, Lenke LG, Jackson R, Newton PO. Three-dimensional analysis of thoracic apical sagittal alignment in adolescent idiopathic scoliosis. Spine. 2009;34(8):792–797.

He C, To MK, Cheung JP, Cheung KM, Chan CK, Jiang WW, Zhou GQ, Lai KK, Zheng YP, Wong MS. An effective assessment method of spinal flexibility to predict the initial in-orthosis correction on the patients with adolescent idiopathic scoliosis (AIS). PLoS One. 2017;12(12):e0190141.

Herzenberg JE, Waanders NA, Closkey RF, Schultz AB, Hensinger RN. Cobb angle versus spinous process angle in adolescent idiopathic scoliosis. The relationship of the anterior and posterior deformities. Spine. 1990;15(9):874–879.

Huang QH, Zheng YP, Lu MH, Chi ZR. Development of a portable 3D ultrasound imaging system for musculoskeletal tissues. Ultrasonics. 2005;43(3):153–163.

Jiang WW, Cheng CLK, Cheung JPY, Samartzis D, Lai KKL, To MKT, Zheng YP. Patterns of coronal curve changes in forward bending posture: a 3D ultrasound study of adolescent idiopathic scoliosis patients. Eur Spine J. 2018 ;27(9):2139-2147.

Knott P, Mardjetko S, Nance D, Dunn M. Electromagnetic topographical technique of curve evaluation for adolescent idiopathic scoliosis. Spine 2006;31(24):E911-5

Lewis JS, Valentine RE. Clinical measurement of the thoracic kyphosis. A study of the intra-rater reliability in subjects with and without shoulder pain. BMC Musculoskelet Disord 2010;11:39.

Li M, Cheng J, Ying M, Ng B, Zheng Y, Lam T, Wong W, Wong M. Could clinical US improve the fitting of spinal orthosis for the patients with AIS? Eur Spine J. 2012;21(10):1926–1935.

Mannion AF, Knecht K, Balaban G, Dvorak J, Grob D. A new skin-surface device for measuring the curvature and global and segmental range of motion of the spine: reliability of measurements and comparison with data reviewed from the literature. Eur Spine J. 2004;13(2):122–136.

Marks M, Stanford C, Newton P. Which lateral radiographic positioning technique provides the most reliable and functional representation of a patient's sagittal balance? Spine. 2009;34(9):949–954.

McKenna C, Wade R, Faria R, Yang H, Stirk L, Gummerson N, Sculpher M, Woolacott N. EOS 2D/3D X-ray imaging system: a systematic review and economic evaluation. Health Technol Assess. 2012;16(14):1–188.

Pasha S, Capraro A, Cahill PJ, Dormans JP, Flynn JM. Bi-planar spinal stereoradiography of adolescent idiopathic scoliosis: considerations in 3D alignment and functional balance. Eur Spine J. 2016;25(10):3234–3241.

Pope MH, Stokes IAF, Moreland M. The biomechanics of scoliosis. CRC Crit Rev Biomed Eng. 1984;11:157–188.

Post M, Verdun S, Roussouly P, Abelin-Genevois K. New sagittal classification of AIS: validation by 3D characterization. Eur Spine J 2019.

Pruijs JE, Hageman MA, Keessen W, van der Meer R, van Wieringen JC. Variation in Cobb angle measurements in scoliosis. Skeletal Radiol. 1994;23(7):517-20.

Ronckers CM, Land CE, Miller J, Stovall M, Lonstein JE, Doddy MM. Cancer mortality among women frequently exposed to radiographic exams for spinal disorders. Radiat Res. 2010;174(1):83–90.

Salem W, Coomans Y, Brismée JM, Klein P, Sobczak S, Dugailly PM. Sagittal Thoracic and Lumbar Spine Profiles in upright standing and Lying Prone Positions among Healthy Subjects: Influence of various Biometric features. Spine 2015.

Salman A, Arzola C, Tharmaratnam U, Balki M. Ultrasound imaging of the thoracic spine in paramedian sagittal oblique plane: the correlation between estimated and actual depth to the epidural space. Reg Anesth Pain Med. 2011;36(6):542–547.

Schlösser TP, Shah SA, Reichard SJ, Rogers K, Vincken KL, Castelein RM. Differences in early sagittal plane alignment between thoracic and lumbar adolescent idiopathic scoliosis. Spine J. 2014;14(2):282–290.

Schmid S, Studer D, Hasler CC, Romkes J, Taylor WR, Brunner R, Lorenzetti S. Using Skin Markers for Spinal Curvature Quantification in Main Thoracic Adolescent Idiopathic Scoliosis: An Explorative Radiographic Study. PLoS One. 2015;10(8):e0135689

Schmitz-Feuerhake I, Pflugbeil S. 'Lifestyle' and cancer rates in former East and West Germany: the possible contribution of diagnostic radiation exposures. Radiat Prot Dosimetry. 2011;147(1–2):310–313.

Shrout PE, Fleiss JL. Intraclass correlations: uses in assessing rater reliability. Psychol Bull. 1979;86(2):420–428.

Simony A, Hansen EJ, Christensen SB, Carreon LY, Andersen MO. Incidence of cancer in adolescent idiopathic scoliosis patients treated 25 years previously. Eur Spine J 2016;25(10):3366-3370.

Sullivan TB, Reighard FG, Osborn EJ, Parvaresh KC, Newton PO. Thoracic Idiopathic Scoliosis Severity Is Highly Correlated with 3D Measures of Thoracic Kyphosis. J Bone Joint Surg Am. 2017;99(11):e54.

Suzuki S, Yamamuro T, Shikata J, Shimizu K, Iida H. Ultrasound measurement of vertebral rotation in idiopathic scoliosis. J Bone Joint Surg Br 1989;71(2):252-255

Tambe AD, Panikkar SJ, Millner PA, Tsirikos AI. Current concepts in the surgical management of adolescent idiopathic scoliosis. Bone Joint J. 2018;100-B(4):415-424.

Timothy Tin Yan Lee, James Chung Wai Cheung, Yen Law, Michael Kai Tsun To, Jason Pui Yin Cheung, Yong Ping Zheng. Analysis of Sagittal Profile of Spine Using 3D Ultrasound Imaging: A Phantom Study and Preliminary Subject Test. CMBBE: Imaging & Visualiation 2019.

Ungi T, King F, Kempston M, Keri Z, Lasso A, Mousavi P, Rudan J, Borschneck DP, Fichtinger G. Spinal curvature measurement by tracked US snapshots. US Med Biol. 2014;40(2):447–454.

Vrtovec T, Pernus F, Likar B. A review of methods for quantitative evaluation of spinal curvature. Eur Spine J. 2009;18:593–607.

Wang Q, Li M, Lou EH, Wong MS. Reliability and Validity Study of Clinical Ultrasound Imaging on Lateral Curvature of Adolescent Idiopathic Scoliosis. PLoS One 2015;10(8):e0135264.

Young M, Hill DL, Zheng R, Lou E. Reliability and accuracy of US measurements with and without the aid of previous radiographs in adolescent idiopathic scoliosis (AIS). Eur Spine J. 2015;24(7):1427–1433.

Zheng YP, Lee TT, Lai KK, Yip BH, Zhou GQ, Jiang WW, Cheung JC, Wong MS, Ng BK, Cheng JC, Lam TP. A reliability and validity study for Scolioscan: a radiation-free scoliosis assessment system using 3D ultrasound imaging. Scoliosis Spinal Disord. 2016;11:13.

Zhou GQ, Jiang W, Lai KL and Zheng YP. Automatic Measurement of Spine Curvature on 3-D Ultrasound Volume Projection Image With Phase Features. *IEEE Transactions on Medical Imaging*. 2017;36(6): 1250–1262

FIGURE CAPTION LIST

(a) (b)

Figure 1 The diagram illustrates the (a) 3D ultrasound device used in this study and (b) subject being scanned using Scolioscan ultrasound system in natural standing posture

Figure 2 The diagram shows the measurement of coronal ultrasound angle(s) on the coronal image

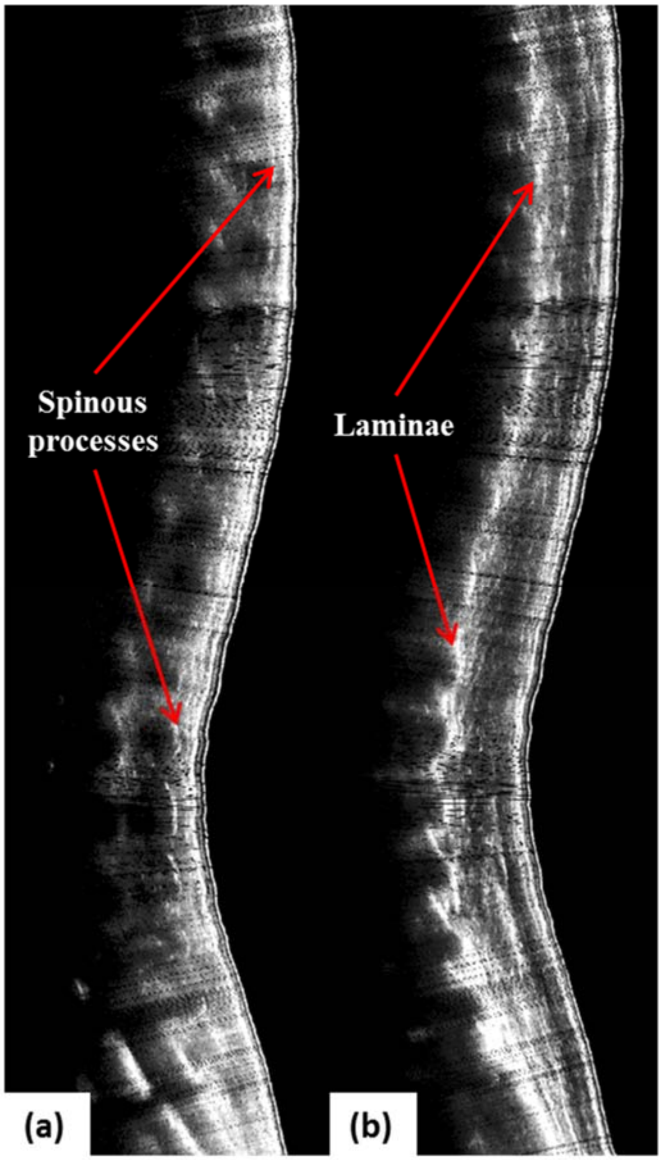

Figure 3. The diagram shows a sagittal ultrasound sagittal image illustrating (a) spinous processes and (b) lateral laminae.

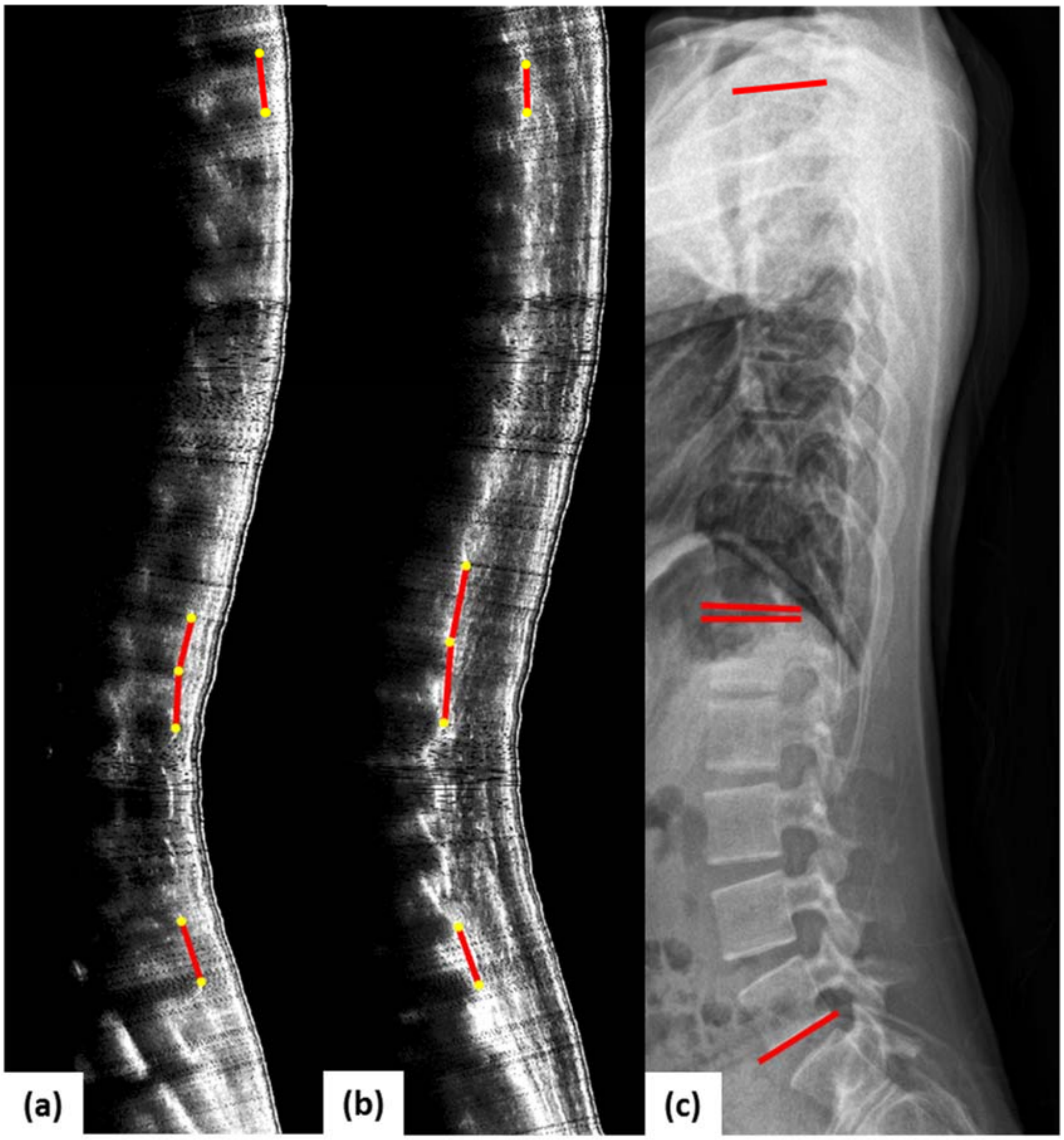

Figure 4. The diagram shows the measurement of (a) ultrasound spinous process angle (USSPA), (b) ultrasound laminae angle (USLA) and (c) Cobb's angle (XCA) for evaluating thoracic kyphosis and lumbar lordosis respectively.

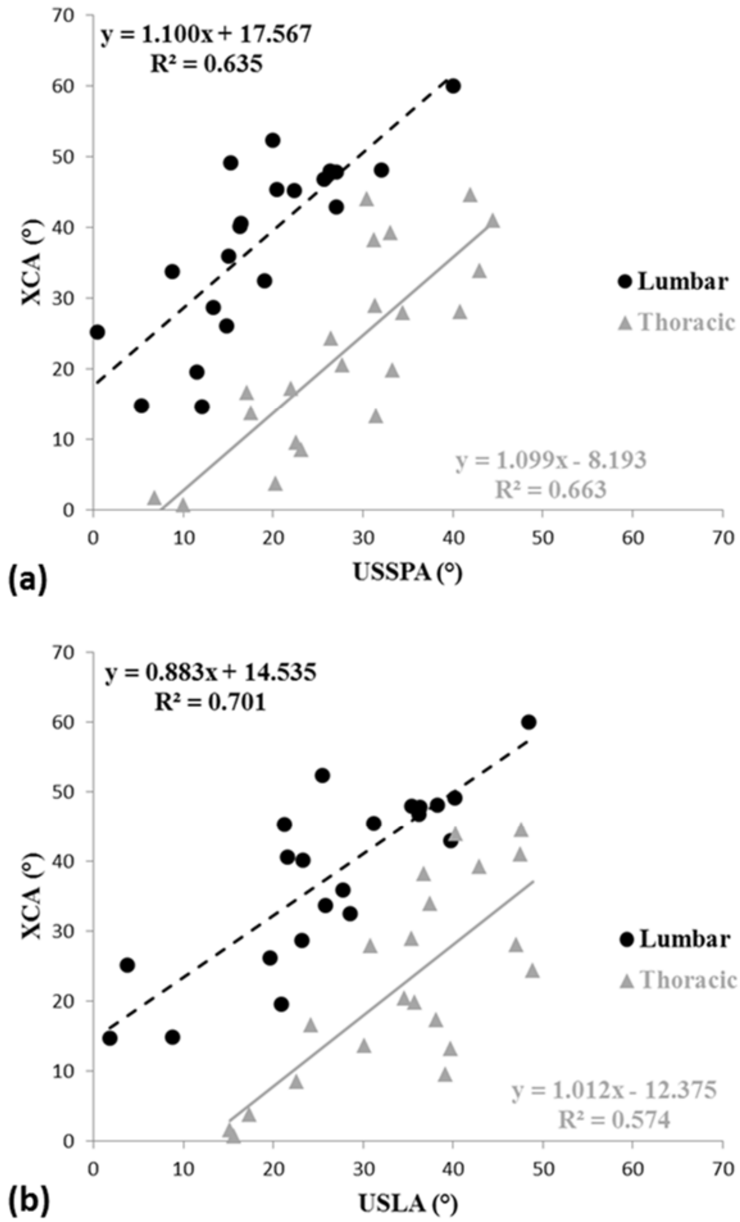

Figure 5. The graphs show the correlations (R^2) and equations between the X-ray Cobb's angles (XCA) and the ultrasound angles based on (a) spinous processes (USSPA) and (b) laminae (USLA) of the thoracic (grey) and lumbar (black) curves.

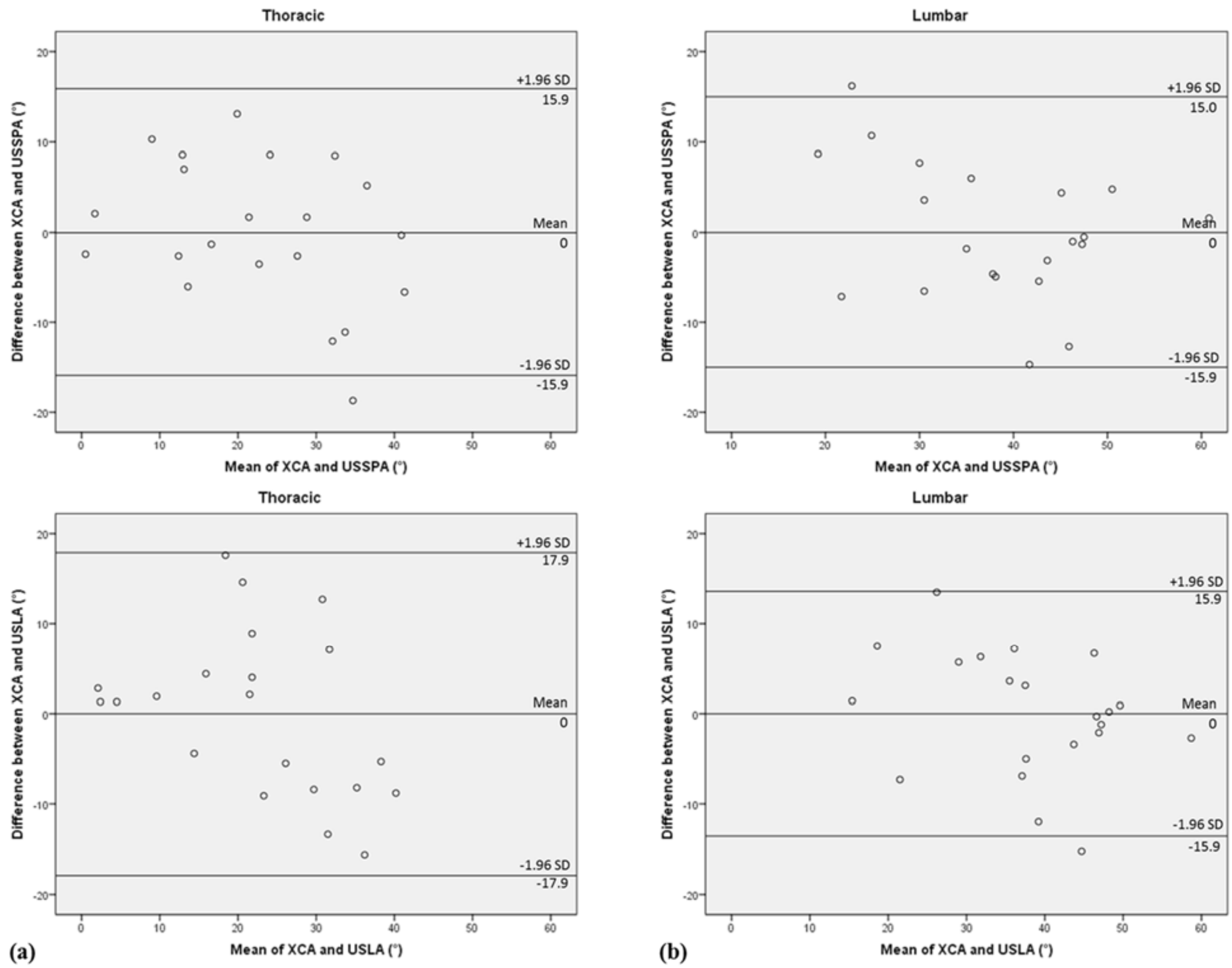

Figure 6. The Bland-Altman plots which shows the differences between X-ray Cobb's angles (XCA) and the sagittal ultrasound angles (USSPA and USLA respectively) corrected with the linear regression equations of the (a) thoracic and (b) lumbar regions respectively. SD: standard deviation.

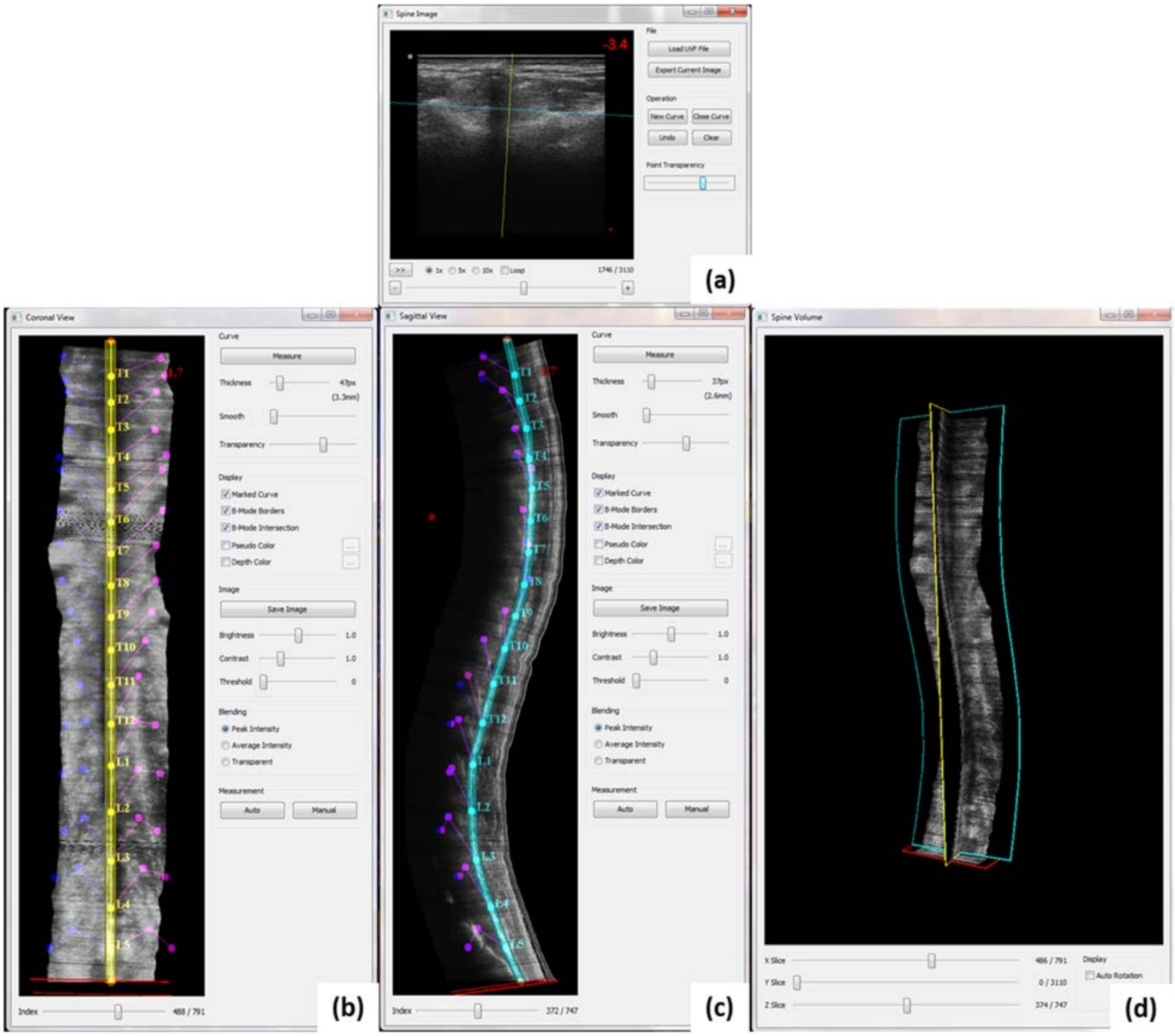

Figure A.1. The diagram which shows the components of the customized 3D software used in this study to generate optimal sagittal images for sagittal curvature analysis: a) B-mode image window; b) Coronal plane images window; c) Sagittal image window; and d) Overall ultrasound volume window with all three planes.

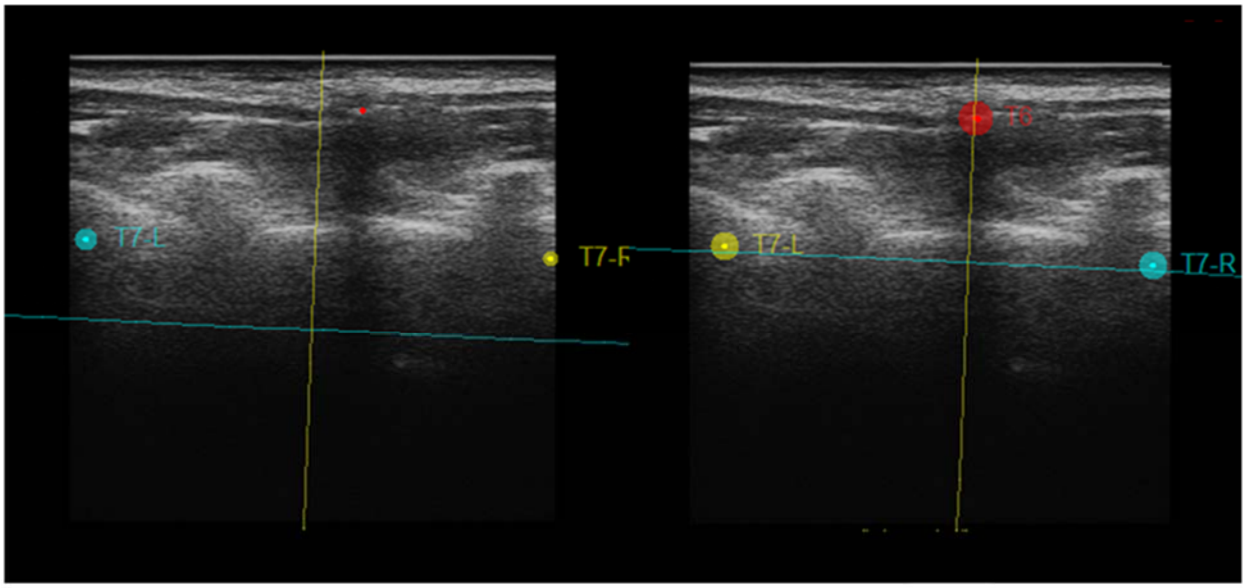

(a) (b)

Figure A.2 The diagram which shows a) the temporary marker attached to the T6 spinous process and b) the corresponding T6 marker in the marker point set was manually dragged to the location of the temporary marker, making the customized cut plane align with the spinous process.

Figure B.1 The diagram which shows the measurement of centre of posterior tangent Angle (XPTA) for evaluating thoracic kyphosis and lumbar lordosis respectively.

Table 1. Intra-rater and inter-rater reliability of the sagittal ultrasound angles by Rater 1 and Rater 2.

Angle	Curve	Rater 1 Intra ICC	Rater 2 Intra ICC	First measurement Inter ICC
USSPA	Thoracic	0.98 (0.96 – 0.99)	0.93 (0.84 – 0.97)	0.95 (0.87 – 0.98)
	Lumbar	0.96 (0.91 – 0.98)	0.92 (0.81 – 0.97)	0.94 (0.86 – 0.98)
USLA	Thoracic	0.99 (0.96 – 0.99)	0.97 (0.92 – 0.99)	0.95 (0.88 – 0.98)
	Lumbar	0.98 (0.94 – 0.99)	0.97 (0.92 – 0.98)	0.94 (0.40 – 0.98)

**ICC: Intraclass correlation coefficient; USSPA: Ultrasound spinous process angle; USLA: Ultrasound laminae angle; Parentheses represent the 95% confidence interval for the coefficient*

Table 2. Intra-rater reliability of the sagittal ultrasound angles measured by Rater 1 from different ultrasound sagittal images generated using the customized 3D software from the same scan

Angle	Curve	Rater 1 Intra ICC
USSPA	Thoracic	0.95 (0.91 – 0.98)
	Lumbar	0.91 (0.84 – 0.96)
USLA	Thoracic	0.96 (0.90 – 0.98)
	Lumbar	0.93 (0.84 – 0.97)

**ICC: Intraclass correlation coefficient; USSPA: Ultrasound spinous process angle; USLA: Ultrasound laminae angle; Parentheses represent the 95% confidence interval for the coefficient*

APPENDIX A

After the 3D ultrasound volume was collected for the patient, it was then transferred to the customized 3D software for further processing. For coronal images, back surfaces of the patients are used as the reference for forming the sagittal cut plane before performing volume projection imaging, to form the coronal images (Zheng et al. 2016). However, the coronal cut planes, which are needed to generate the sagittal images which illustrates the spinous processes (Figure 3a) and bilateral laminae (Figure 3b), required manual formation. The 3D software allows the user to view the B-mode images with marked frame numbers, the coronal and sagittal views of the ultrasound volume and the three planes over the entire volume (Figure A.1). From the coronal and sagittal view windows of the 3D software, a marker set model and an intersection frame also appear in both windows (Yellow and blue in coronal and sagittal view respectively) (Figure A.1b and A.1c). The coronal intersection frame in the coronal window projects the sagittal image in the sagittal window and vice versa. The position of the markers on the marker set model of each window can be manually deformed and the shape of the intersection frame will change simultaneously, eventually the corresponding projected images in both planes.

An algorithm developed in previous study (Zhou et al. 2017), which allows auto-detection of the spinous process shadow of the coronal images, was embedded in the 3D software and employed to coarsely form the coronal cut plane illustrating the spinous processes. The shadow of the ribs appeared in the coronal image from the coronal window allow the user to identify the T12 vertebrae. With the view of the coronal and sagittal projected images and the raw B-mode images from the 3D software and the knowledge of the posterior anatomy of the thoracic and lumbar vertebrae, individual spinous process and bilateral laminae in each vertebral level could also be identified. After identifying the best frames that illustrate the spinous process and bilateral laminae of each laminae from the B-mode images, the corresponding markers from the marker set model could be dragged to the vertebrae structures (Figure A.2). This dragging procedure is facilitated by a function embedded in the 3D software, where a temporary marker could be set on the B-mode image and could be seen on the coronal and sagittal images. Generally, spinous processes appear under the spinous process shadow and bilateral laminae appear bilaterally next to the spinous process shadow. Hence by repeating the above procedures, the manually defined coronal cut planes which align with the spinous processes (Figure A.3a) and bilateral laminae (Figure A.3b: left laminae and A.3c right laminae) could be formed and the corresponding sagittal images were outputted for analysis (Figure A.3d, A.3e and A.3f).

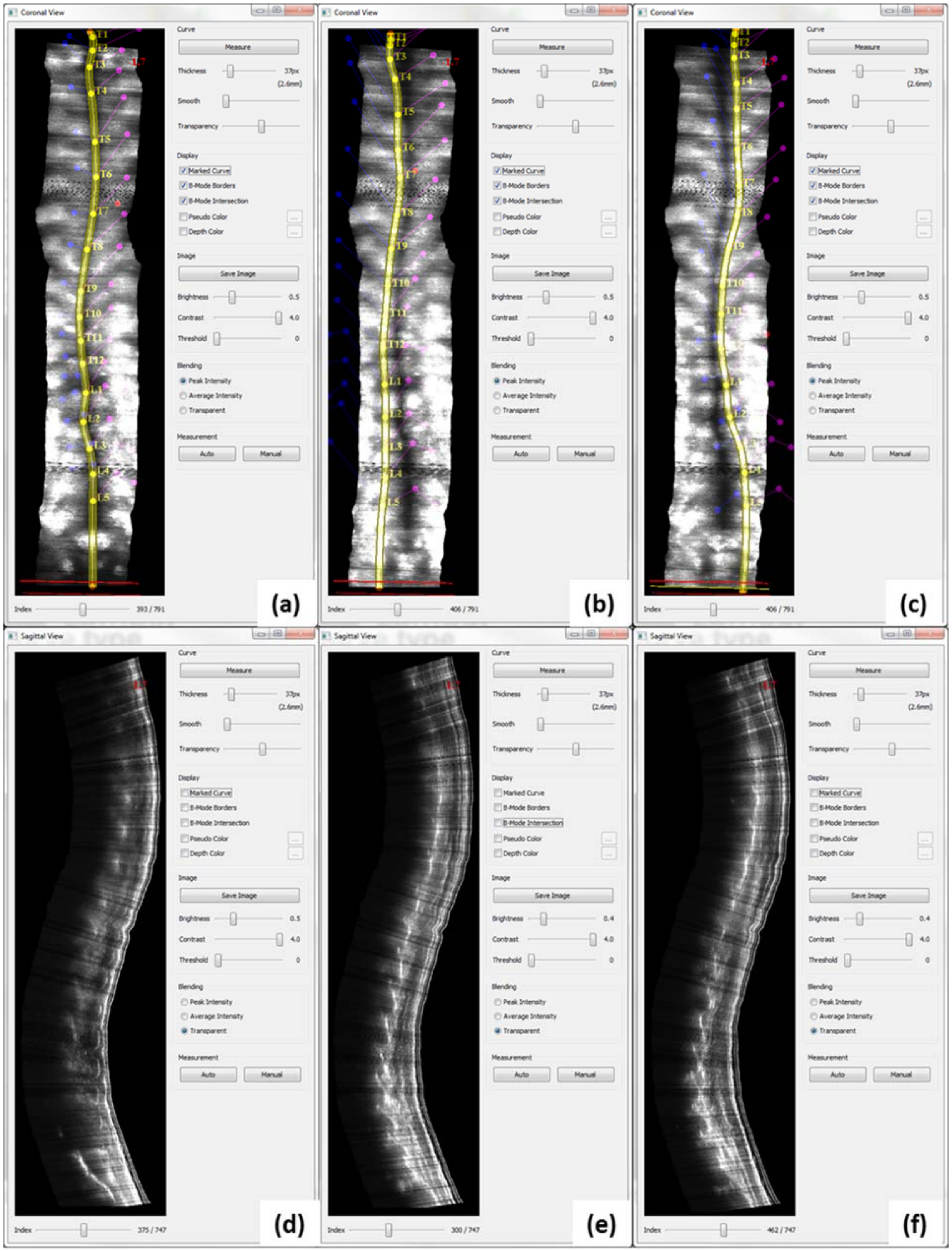
Coronal View
Curve
Measure
Thickness
Smooth
Transparency
Display
Marked Curve
B-Mode Borders
B-Mode Intersection
Pseudo Color
Depth Color
Image
Save Image
Brightness
Contrast
Threshold
Blending
Peak Intensity
Average Intensity
Transparent
Measurement
Auto
Manual
Index
(a)
(b)
(c)
Sagittal View
(d)
(e)
(f)

Figure A.3.

APPENDIX B

An extra set of X-ray measurements, called the Centre of Posterior Tangent Angle (XPTA), was measured in order to explore and demonstrate the effect of different structures and measurement techniques on sagittal measurements, which is based on the posterior tangent method by Harrison et al. (1996). For XPTA, thoracic kyphosis was defined by the angle formed between the line joining the centre of T3 and T4 posterior border and the line joining the centre of T11 and T12 posterior border, whereas lumbar lordosis was defined by the intersection angle between the line joining the centre of T12 and L1 posterior border and the line joining the centre of L4 and L5 posterior border (Figure B.1). All the measurements were performed using RadiAnt DICOM Viewer software (Medixant, Poland) and were shown in Table B.1. It could be observed that there was a clinically significant difference between the XCA and XPTA, and XPTA obtained had a smaller angular difference with USLA and USSPA compared to XCA.

Table B.1 *Mean value of thoracic kyphosis and lumbar lordosis obtained from four different methods using X-ray and ultrasound respectively.*

	X-ray		**Ultrasound**	
	XCA	**XPTA**	**USLA**	**USSPA**
TK (º)	22.7 ± 14.0	30.0 ± 13.1	34.2 ± 10.7	28.1 ± 10.4
LL (º)	38.0 ± 12.6	28.9 ± 11.9	27.1 ± 12.1	18.5 ± 9.2

XCA:X-ray Cobb angle; XPTA: X-ray centre of posterior tangent angle; USLA: Ultrasound laminae angle; USSPA: Ultrasound spinous process angle; TK: Thoracic kyphosis; LL: Lumbar lordosis